Langmuir

ARTICLE

pubs.acs.org/Langmuir

Amphiphilic Silica Nanoparticles at the Decane−Water Interface: Insights from Atomistic Simulations

Heng Fan, Daniel E. Resasco, and Alberto Striolo*

School of Chemical, Biological, and Materials Engineering, The University of Oklahoma, Norman, Oklahoma 73019, United States

Supporting Information

ABSTRACT: The properties of 3 nm-diameter silica nanoparticles with different surface chemistry were systematically investigated at the decane−water interface using molecular dynamics simulations. Our results show that the decane−water interfacial tension is not much influenced by the presence of the nanoparticles. The three-phase contact angle increases with nanoparticle surface hydrophobicity. Contact angles observed for the nanoparticles at 300 and at 350 K differ very little. The contact angle of the nanoparticle with randomly dispersed hydrophobic groups is smaller than that observed in Janus nanoparticles of equal overall surface chemistry composition. The energy necessary to desorb Janus nanoparticles from the interface is usually higher than that required to desorb the corresponding homogeneous nanoparticles. Desorption from the interface into the aqueous phase is preferred over that into the organic phase for all except one of the nanoparticles considered. Structural and dynamic properties including nanoparticle rotational relaxation, solvent density profiles, and solvent residence autocorrelation functions near the nanoparticles are also presented. The data are useful for designing Pickering emulsions.

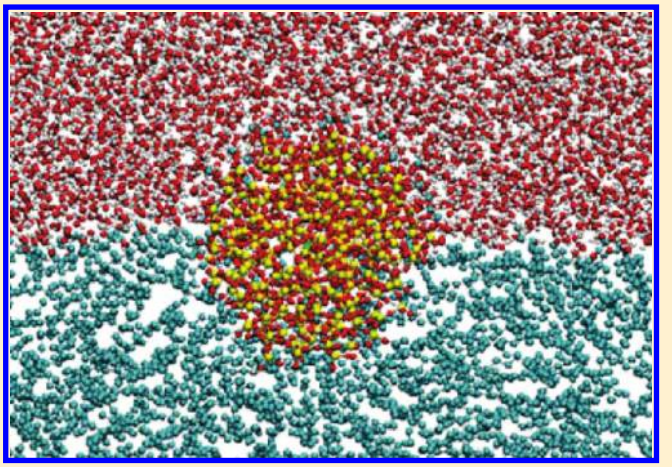

1. INTRODUCTION

Energy sources alternative to fossil fuels are required to maintain, and keep expanding, our standards of living. Large public attention and research efforts are being devoted to biofuels. Among numerous procedures to produce biofuels from biomass, pyrolysis is a promising approach.[1] This procedure has several inherent advantages, including the fact that expensive and delicate fermentation processes are not required, it is fast, and it can be applied to several biomass sources including switch grass. The main limitation encountered by pyrolysis is that the bio-oil obtained is a complex fluid that contains up to 30% water.[1] Refining this fluid using traditional chemical engineering techniques requires multiple steps to separate out hydrophilic byproduct incompatible with fuel applications.[2] The sequential catalytic reactions needed to upgrade the bio-oil could be conducted under phase-transfer conditions within the as-produced biooil, before undergoing separations.[3] For such an approach to be feasible, one requires biphasic systems with large interfacial area. Stable emulsions of water droplets finely dispersed in the oil phase are one such system. Solid nanoparticles could play the role of stabilizing agents, yielding Pickering emulsions.[4] Appropriately designed solid nanoparticles could yield stable water-in-oil emulsions, support heterogeneous catalysts, and could also be recovered via filtration after the biooil has been upgraded.

As extensively demonstrated by Binks and collaborators,[5−7] solid nanoparticles with different inherent wettability can be used to stabilize different types of emulsions. The wettability of a nanoparticle can be tuned by grafting appropriate hydrophilic vs hydrophobic groups on the nanoparticle surface. Janus nanoparticles, which present two surface regions with different wettability, have been found to better stabilize emulsions, presumably because of the larger desorption energy necessary to displace such nanoparticles from the interface compared to that required to remove homogeneous nanoparticles.[8]

Despite these useful general principles and despite some recently developed experimental techniques,[9−11] it remains difficult to study the properties of nanoparticles at oil−water interfaces solely via experiments. Herein we report molecular dynamics (MD) simulations attempting to unveil the intrinsic molecular level behavior of amphiphilic silica nanoparticles at the water−decane interface.

2. METHODOLOGY

Simulated spherical amorphous silica nanoparticles were prepared as follows. Bulk amorphous silica was generated from a melt-quench process as proposed by Litton et al.[12] From the amorphous material, a spherical nanoparticle of desired diameter was carved out. For practical applications, it would be desirable to consider large particles, up to a few

Received: February 1, 2011
Revised: March 14, 2011
Published: March 30, 2011

Table 1. Type, Geometry, and Surface Chemistry of the Seven Nanoparticles Simulated[a]

nanoparticles	HP-1	HP-2	HP-3	HP-4	JP-1	JP-2	JP-3
surface group composition	100% OH	100% CH_3	58% CH_3 42% OH	62%CH_3 38% OH	58% CH_3 42% OH	16% CH_3 84% OH	62% CH_3 38% OH
α	N/A	N/A	N/A	N/A	90°	37°	100°
				106 total surface groups, 38 (36%) germinal; R = 1.5 nm			

[a] The geometric angle α quantifies the boundary dividing hydrophobic from hydrophilic surface regions, as shown illustratively in Figure 3. The radius of the nanoparticle, R, is calculated by averaging the distance between all the non-bridging oxygen atoms and the nanoparticle geometric center.

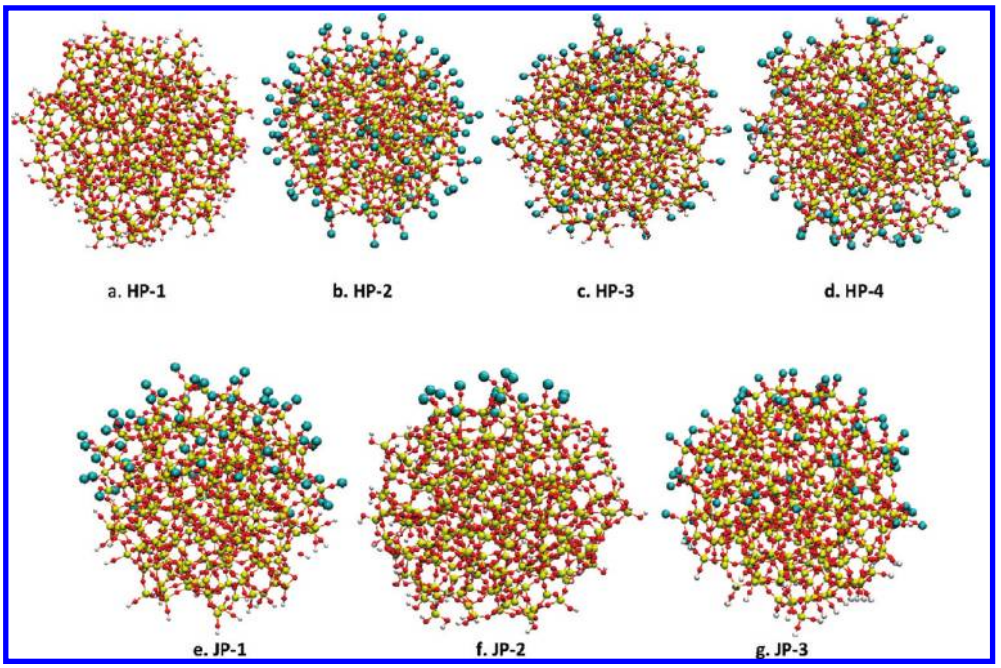

Figure 1. Nanoparticles simulated in this work. Blue, yellow, white, and red spheres represent CH_3 united atoms, silicon, hydrogen, and oxygen atoms, respectively. (a) HP-1: homogeneous nanoparticle covered by hydrophilic OH groups. (b) HP-2: homogeneous nanoparticle fully covered by hydrophobic CH_3 groups. (c) HP-3: homogeneous nanoparticle randomly covered by 58% CH_3 groups and 42% OH groups. (d) HP-4: homogeneous nanoparticle randomly covered by 62% CH_3 groups and 38% OH groups. (e) JP-1: Janus nanoparticle covered by 58% CH_3 groups and 42% OH groups. (f) JP-2: Janus nanoparticle covered by 16% CH_3 groups and 84% OH groups. (g) JP-3: Janus nanoparticle covered by 62% CH_3 groups and 38% OH groups.

micrometers in diameter. For economy of computational resources, small particles as little as one nanometer in diameter are instead desirable. As a compromise, all the nanoparticles simulated in this work are of 3 nm in diameter. Unsaturated silica atoms were removed from the nanoparticle surface and the nonbridging oxygen atoms were saturated with either one hydrogen atom (yielding hydroxyl groups), or with one methyl group. Nanoparticles of different hydrophobicity were constructed by tuning the ratio of hydroxyl to methyl groups on the nanoparticle surface (hydrophilic and hydrophobic, respectively).

In Table 1 and Figure 1, we report detailed information regarding the nanoparticles considered in this study. In all cases the surface density of functional groups is 4.5 groups/nm^2, which agrees with experimental data obtained on flat amorphous silica (4.6 OH groups/nm^2).[13] Out of the total 106 surface groups present on one nanoparticle, 38 are germinal. Seven nanoparticles of different surface chemistry were studied. They are the following, as shown in Figure 1: (1) one homogeneous nanoparticle covered by 106 hydrophilic OH groups (HP-1); (2) one homogeneous nanoparticle covered by 106 (100%) hydrophobic CH_3 groups (HP-2); (3) one homogeneous nanoparticle randomly covered by 58% CH_3 groups and 42% OH groups (HP-3); (4) one homogeneous nanoparticle randomly covered by 62% CH_3 groups and 38% OH groups (HP-4); (5) one Janus nanoparticle covered by 58% CH_3 groups and 42% OH groups (JP-1); (6) one Janus nanoparticle covered by 16% CH_3 groups and 84% OH groups (JP-2); and (7) one Janus nanoparticle covered by 62% CH_3 groups and 38% OH groups (JP-3). For completeness, we point out that the CH_3 groups substituted the hydrogen atoms on the surface OH groups, thus Si−O−CH_3 bonds are present on hydrophobic and partially hydrophobic nanoparticle surfaces

To build the systems containing water, decane, and one nanoparticle, shown in Figure 2, we first equilibrated a large rectangular simulation cell, containing water and decane, of dimensions 8 nm × 8 nm × 12 nm at 300 K for 2 ns. Decane formed a layer of 6 nm thickness along the Z direction. After equilibration, a spherical cavity was carved out either at the water−decane interface or within the water phase to insert one nanoparticle. The system was then equilibrated in an *NPT* (constant number of particles, pressure, and temperature) ensemble at P = 1 atm (isotropic pressure coupling was implemented), and T = 300 K or T = 350 K for 8 ns as the total energy and the system volume stabilized. Simulations were then conducted for additional 20 ns in the *NPT* ensemble. The data obtained from the last 10 ns were used to obtain the results presented here. After equilibration changes in interfacial area were within 1%. Decane molecules were found to be isotropically oriented at the center of the decane film, while they were parallel to the interface near the interface. Details are presented as Supporting Information.

The CLAYFF force field[14] was employed to describe the interactions between atoms of silica. The transferable potentials for phase equilibria

dx.doi.org/10.1021/la200428r |*Langmuir* 2011, 27, 5264–5274

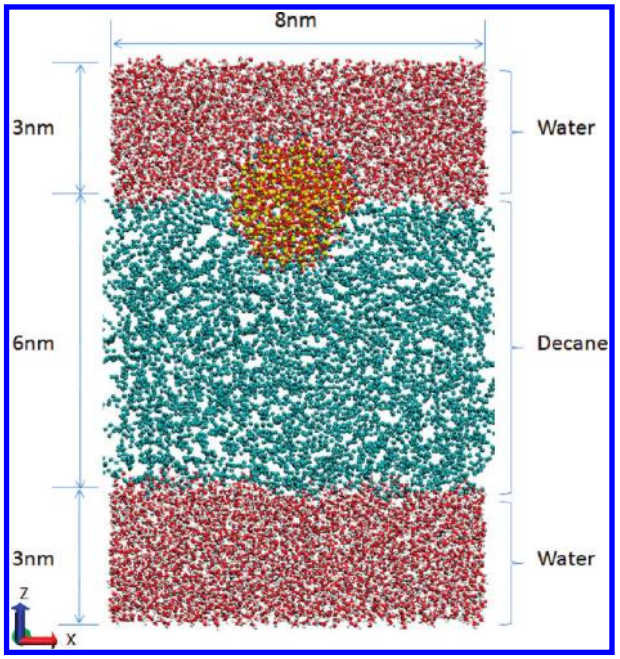

Figure 2. Schematic representation of the simulation box. Blue, yellow, white and red spheres represent CH_3 united atom groups, silicon, hydrogen, and oxygen atoms, respectively.

(TraPPE) force field[15] was employed to model *n*-decane and the alkane groups on the nanoparticle. The single point charge/extended (SPC/E) model was implemented to model water.[16] The atoms of the nanoparticle interact with water and decane via dispersive and electrostatic forces.[17] Dispersive interactions were modeled with a 12−6 Lennard-Jones (LJ) potential. The LJ parameters for unlike interactions were determined using customary Lorentz−Berthelot mixing rules.[18] The particle-mesh Ewald (PME)[18,19] method was used to correct for long-range electrostatic interactions. The cutoff for all interactions was set to 0.9 nm. Interactions between surface groups and other atoms within one nanoparticle were excluded, as required by the CLAYFF force field.[14]

All molecular dynamics (MD) simulations were performed using the GROMACS 4.0.5 package.[20−23] The leapfrog algorithm[18] was used for integrating Newton's equations of motion with a time step of 1 fs. All simulations were carried out under the *NPT* ensemble using the Berendsen thermostat[24] at 300 K or 350 K and 1 bar with 100 fs relaxation time. Periodic boundary conditions were implemented along all three directions. During production, the atomic positions were recorded every 1 ps and used for further analysis.

In most cases, to reduce the computational cost one nanoparticle was simulated at one decane−water interface, while the other decane−water interface was considered without a nanoparticle, as shown in Figure 2. When the decane−water interfacial tension was calculated, two identical nanoparticles were simulated, one on each interface. In this case, the system was equilibrated for 10 ns within the NPT ensemble, followed by 3 ns of production during which the volume was kept fixed (NVT ensemble). The NVT ensemble was implemented only to study interfacial tension.

The desorption energy was obtained by computing the energy required to pull one adsorbed nanoparticle away from the interface into one phase, using an umbrella spring. We employed the center of mass pulling algorithm as available in GROMACS 4.0.5. Within this algorithm, the position of the center of mass of the nanoparticle was forced to move at constant velocity (pulling rate) from the interface to the bulk of either one of the two phases at contact. A harmonic spring ensured that the center of mass oscillated around the desired position. A simulation box of dimensions 6 nm × 6 nm × 19 nm, in which decane formed a 9 nm thick layer, was used for these calculations. The harmonic force constant for the spring was set to 300 000 kJ/(mol·nm), stiff enough to mimic a process with constant 1 nm/ns pulling rate. At each position of the nanoparticle center of mass with respect to the water−decane interface, the resultant force acting on the nanoparticle center of mass because of neighboring water and decane molecules was recorded. The desorption energy was then obtained, as described in more details later, by integrating the force along the distance from the interface. These simulations are conducted within the *NPT* ensemble.

Table 2. Simulation Results for Interfacial Tension, Compared to Available Experimental Data[28]

	γ (T = 300 K) mN/m	γ (T = 350 K) mN/m
no particle: simulation	52.7 ± 1.7	43.8 ± 2.4
no particle: experiment[28]	51.7	47.7
HP-2	49.8 ± 0.9	46.7 ± 0.9
HP-3	50.9 ± 0.9	46.3 ± 1.8
HP-4	51.4 ± 5.4	40.9 ± 2.3
JP-1	51.3 ± 1.6	44.2 ± 0.7
JP-2	49.8 ± 1.0	44.7 ± 1.9
JP-3	53.3 ± 3.0	44.1 ± 2.6

3. RESULTS AND DISCUSSION

The HP-1 nanoparticle, which is completely covered by hydrophilic OH groups (see Figure 1, panel a), partitions preferentially in the aqueous phase at both temperatures considered (300 and 350 K). This is consistent with experiments by Ohtani et al.,[25] which show that hydrophilic silica nanoparticles are not suitable for stabilizing either oil in water (o/w) or water in oil (w/o) emulsions. All other simulated nanoparticles preferentially reside at the water−decane interface both at 300 and 350 K. This suggests that these nanoparticles could stabilize emulsions, although the type of emulsion stabilized should depend on the three-phase contact angle at the decane−water interface.[5] When the three-phase contact angle is larger than 90°, w/o emulsion are stabilized. When the contact angle is less than 90°, o/w emulsion are stabilized.

3.1. Interfacial Tension. As discussed by Dai and coworkers,[26] to reliably simulate nanoparticles at liquid−liquid interface, it is necessary that the force fields implemented correctly predict the interfacial tension between the liquids in contact. The interfacial tension was calculated using the following equation:[27]

$$\gamma = \frac{1}{2}\left\langle \left(P_{zz} - \frac{P_{xx} + P_{yy}}{2} \right) \right\rangle L_z \qquad (1)$$

In eq 1, $P_{\alpha\alpha}$ is the $\alpha\alpha$ component of the pressure tensor, and L_z is the length of the simulation box perpendicular to the interface. Angular brackets denote ensemble averages. The results of our calculations are shown in Table 2, where extrapolations from available experimental data[28] are also displayed.

The interfacial tension of the decane−water interface (without nanoparticles) was compared to data extrapolated, using a linear correlation on temperature, from the experimental results reported by Zeppieri et al.[29] Both experimental and simulation data, in good agreement, show that the surface tension decreases as the temperature rises. The good agreement between simulated and extrapolated experimental data suggests that the

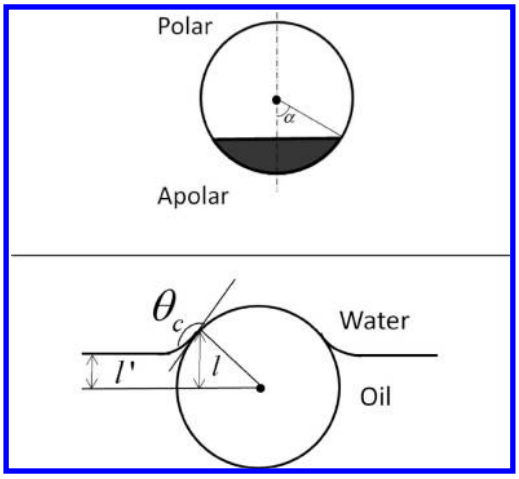

Figure 3. (top) Schematic representation illustrating the geometric angle α used in Table 1 to characterize Janus nanoparticles. (bottom) Schematic illustration for the difference between the contact angles calculated from the position of the water−decane interface and that obtained from the position of the water−decane−nanoparticle interface.

force fields implemented are suitable to study the water−decane interface.

The results observed for the surface tension in the presence of nanoparticles indicate that there is no significant change for the simulated surface tension compared to the value obtained at the water−decane interface without nanoparticles. This agrees with a number of experimental data indicating that nanoparticles adsorb at the interface primarily to reduce the area of the high-energy oil−water interface (see, e.g., the early work of Okubo et al.[30] and that of Vignati et al.[31]), contrary to what is typically observed for surfactants. It should however be pointed out that Glaser et al.[32] reported that iron−gold Janus nanoparticles significantly reduce the water−decane interfacial tension. Our simulations for Janus nanoparticles show only modest reductions of interfacial tension. The qualitative difference between our simulation results and the experimental data of Glaser et al. could be due to the different nanoparticles considered (hydrophilic/hydrophobic silica in this work, iron−gold in ref 31), although it is also possible that force fields developed to reproduce structural properties yield underestimations of changes in interfacial tensions when a surface-active molecule adsorbs onto an interface.[33] It is also worth pointing out that the gold portion of the nanoparticles used by Glaser et al. was rendered more hydrophobic by grafting dodecanthiol and octadecanethiol molecules. It is possible that increasing the length of the hydrophobic moieties (CH_3 groups in the present simulations) will have larger effects on the interfacial tension.

3.2. Three-Phase Contact Angle. The three-phase contact angle θ_c formed at the decane−water interface for each nanoparticle simulated was calculated using the following equation:

$$\theta_c = \arccos\left(\frac{l}{R}\right) \qquad (2)$$

In eq 2, l is the distance between the plane identified by the three-phase contact line and the center of the nanoparticle, and R is the nanoparticle radius. Details are provided schematically in Figure 3. Consistent with literature,[6] l is negative when the nanoparticle center is in the oil phase and positive when it resides in the water phase.

Experimentally, the position of the three-phase contact line is often assumed to correspond to the liquid−liquid interface. Because a small meniscus may form near the nanoparticle, it is possible that the contact angle calculated following the two procedures do not coincide. For completeness, we calculated the contact angle using both eq 2 and $\theta_c' = \text{across}(l'/R)$, where l' is the distance between the liquid−liquid interface and the nanoparticle center. An illustrative schematic is shown in Figure 3, bottom panel. The contact angle θ_c and θ_c' are reported in Table 3.

The three-phase contact line is defined here by the position of the water molecules in contact with both nanoparticle and decane. The water−oil interface is defined following the algorithm proposed by Fernandes et al. and by Jorge et al.[34,35] We show two snapshots, in Figure 4, to highlight the difference between l and l'. The small red and blue spheres in Figure 4 are oxygen atoms of water and CH_3/CH_2 groups of decane, respectively, identified in the interfacial region. Out of the oxygen atoms in contact with decane, those closest to the nanoparticle are used to identify the three-phase contact line (big green spheres surrounding the nanoparticle). The green mesh is the plane identified by the three-phase contact line obtained averaging the z coordinates of the oxygen atoms of the water molecules identified by the green spheres in Figure 4. l is the distance between the center of the nanoparticle and this plane. The blue mesh identifies the liquid−liquid interface, from which l' is calculated.

As shown in Table 3, the contact angle calculated from the oil−water interface (θ_c') is sometimes slightly smaller than the contact angle calculated from the three-phase contact line (θ_c), except for nanoparticles HP-3 and HP-4. The small difference between θ_c and θ_c' is mainly due to local density fluctuations, as shown in Figure 4.

An important result from Table 3 is that θ_c for Janus nanoparticles is always several degrees larger than the geometry angle α. This difference, relatively small when the simulation uncertainty is considered, is probably due to the inhomogeneous distribution of surface groups.

In Figure 5, we report the three-phase contact angles θ_c obtained from our simulations as a function of the percentage of methyl groups on the nanoparticle surface. When the ratio equals 0, the nanoparticle is completely hydrophilic (only OH groups on the surface). When the ratio equals 1, the nanoparticle is completely covered by CH_3 groups. When the nanoparticle has no methyl groups, it remains in the water phase and no contact angle can be measured. As shown in Figure 5, the three-phase contact angle increases as the percent of CH_3 groups on the surface increases, for both homogeneous and Janus nanoparticles. For the nanoparticles considered here, it is not possible to obtain a three-phase contact angle larger than ∼105° with Janus nanoparticles (simulation results for Janus nanoparticle with geometric angle α = 105°, not shown for brevity, show a three-phase contact angle of ∼100°), while the homogeneous nanoparticle HP-2, which is completely covered with CH_3 groups, yields a three-phase contact angle of ∼105° at 300 K.

It is expected that the type of emulsion stabilized by nanoparticles (w/o vs o/w) is directly related to the three-phase contact angle.[5] If θ_c is larger than 90°, the nanoparticle tends to stabilize w/o emulsions. If θ_c is less than 90°, the nanoparticle should stabilize o/w emulsions. The dashed line in Figure 5 is used to discriminate between nanoparticles that are expected to stabilize o/w emulsions (JP-2, HP-3, HP-4) and those that

Table 3. Three-Phase Contact Angles Obtained from Simulations[a]

	HP-2	HP-3	HP-4	JP-1	JP-2	JP-3
θ_c (300 K)	104° ± 5	58° ± 4	54° ± 4	95° ± 4	43° ± 4	104.5° ± 4
θ_c' (300 K)	94° ± 4	59° ± 4	53° ± 4.5	86° ± 4	32° ± 7	91.5° ± 3
θ_c (350 K)	107° ± 6	60° ± 5	54° ± 5	95° ± 5	43° ± 4	102° ± 5
θ_c' (350 K)	98° ± 5	59° ± 5	54° ± 6	86° ± 4	33.5° ± 10	90° ± 3

[a] The average contact angle and the errors are measured within 2000 frames of simulation snapshots after the nanoparticles are equilibrated at the interface.

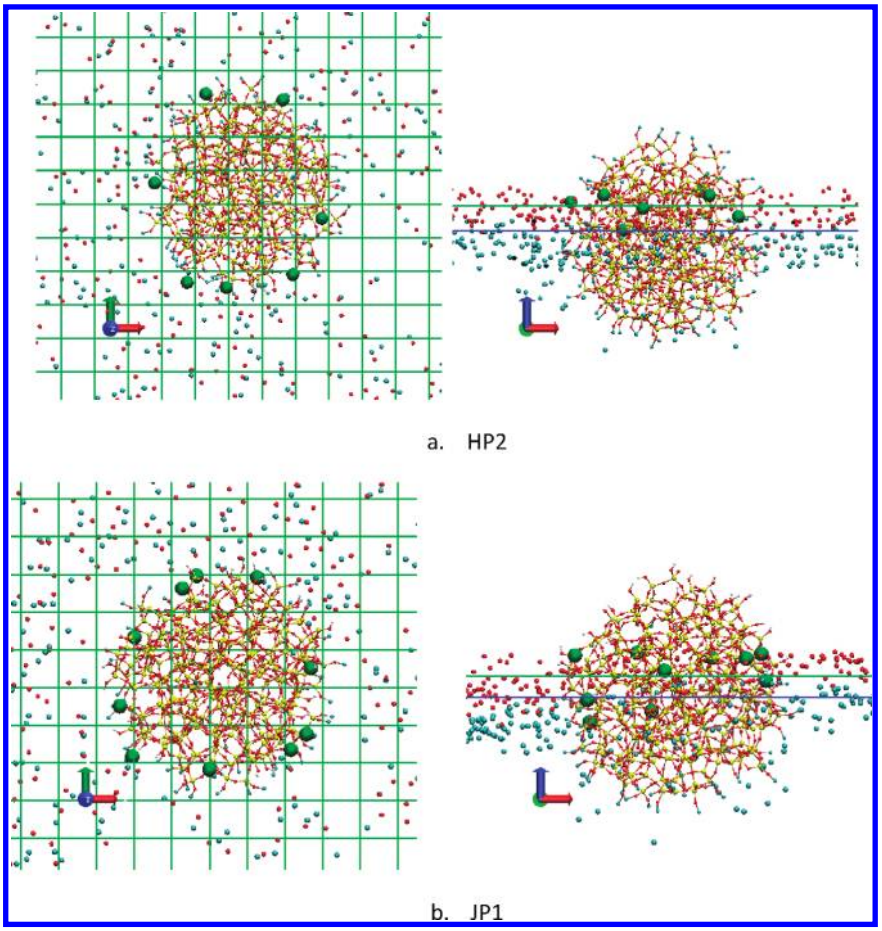

Figure 4. Illustration of the algorithm employed to calculate the contact angle θ_c and θ_c'. Left panels are top views, and right panels are side views. Red and blue spheres identify the interfacial layer of oxygen atoms and decane CH_3/CH_2 united atoms, respectively. Large green spheres represent interfacial water oxygen atoms. The green mesh indicates the plane where the three phase contact line is located, which is calculated by averaging the *z* coordinates of the green spheres. The blue mesh indicates the plane of two phase interface, which is calculated by averaging the z coordinates of oxygen atoms and CH_3/CH_2 united atoms in the interfacial layer.

should stabilize w/o emulsions (HP-2 and JP-3). JP-1 nanoparticles yield a three-phase contact angle close to 90° and, therefore, are likely to stabilize either o/w or w/o emulsions, depending on system conditions. Our results suggest that temperature, within the range considered, does not have large effects on the contact angle.

It is instructive to compare the three-phase contact angle obtained for the homogeneous nanoparticle HP-4 to that obtained for the Janus nanoparticles JP-3. The overall surface chemical composition of HP-4 and JP-3 nanoparticles is identical (62% of the surface groups are CH_3, 38% are OH). The surface groups are homogeneously distributed on the HP-4 nanoparticle surface, while they are concentrated on the hydrophobic and hydrophilic hemispheres on JP-3. As HP-4 and JP-3 have the same number of hydrophobic CH_3 groups, one could have expected them to have similar three-phase contact angles. On the contrary, our results show large differences in the three-phase contact angle (∼58° for HP-4, ∼105° for JP-3 at 300 K). This difference is significant when one observes that, based on these contact angles, HP-4 nanoparticles will stabilize o/w emulsions, while JP-3 nanoparticles are expected to stabilize w/o emulsions. Similar effects are observed when HP-3 and JP-1 nanoparticles, both of which have 58% of CH_3 surface groups, are compared.

From the above discussion, it appears that the overall surface composition alone does not determine the three-phase contact angle. The relative arrangement of hydrophobic and hydrophilic

groups on the surface has a large effect. This observation appears related to the effect of surface heterogeneous chemistry on interfacial water structure and dynamics. Simulation results on flat surfaces for example show that large hydrophobic patches repel water molecules much more strongly than small ones surrounded by hydrophilic groups.[36] Peculiar hydrogen-bonded structures of interfacial water can in fact yield "bridges" that effectively cover the small hydrophobic regions.[37]

3.3. Desorption Energy. The energy required to remove one nanoparticle from the interface into one of the homogeneous phases at contact (desorption energy) can be calculated using macroscopic arguments when the three-phase contact angle shown in Figure 5 is known. At a first approximation, as discussed by Binks and Lumsdon, for homogeneous nanoparticles the desorption energy only relates to the nanoparticle radius R, the contact angle θ_c, and the water−oil interfacial tension γ_{OW} according to[5]

$$E = \pi R^2 \gamma_{ow} (1 \pm \cos \theta_c)^2 \quad (3)$$

Within parentheses, the sign before the cosine is negative for nanoparticle displacement into the water phase and positive for displacement into the oil phase.

For Janus nanoparticles, as shown by Binks and Fletcher and by Jiang and Granick,[8,38] the desorption energy can be expressed in terms of three angles: θ_p, α, and θ_a. For $\theta_p < \alpha < \theta_a$, it can be shown that

$$E_{oil} = 2\pi R^2 \gamma_{ow} \left[\frac{1}{2} \sin^2 \alpha + \cos \theta_p (1 + \cos \alpha)\right] \quad (4)$$

$$E_{water} = 2\pi R^2 \gamma_{ow} \left[\frac{1}{2} \sin^2 \alpha - \cos \theta_a (1 - \cos \alpha)\right] \quad (5)$$

Equations 4 and 5 are based on the "right way round" assumption,[8] according to which the apolar region of the Janus nanoparticle is entirely in contact with the oil phase and the polar region of the Janus nanoparticle is in contact with the aqueous phase. This assumption appears satisfied to a first approximation as shown in Table 3. θ_p and θ_a are the three-phase contact angles obtained for homogeneous nanoparticles of surface chemistry equal to that of the hydrophilic or hydrophobic portion of the Janus nanoparticle, respectively. In our case, for Janus nanoparticles JP-1, JP-2, and JP-3, θ_p should equal the contact angle of HP-1, which cannot be defined because HP-1 nanoparticles preferentially partition to the water phase. We arbitrarily set this value at 0°. For all the Janus nanoparticles considered, θ_a equals the contact angle obtained for HP-2 (e.g., 104° at 300 K). Results for desorption energies calculated from eqs 3, 4, and 5 are reported in Table 4.

For completeness, we also estimated the desorption energy directly from simulations.

In Figure 6, the mechanical energy spent to pull each simulated nanoparticle from the interface to either the aqueous (right) or the organic phase (left) is plotted as a function of the distance from the interface. This mechanical "experiment" starts with the nanoparticle adsorbed in its equilibrium position at the interface. The center of mass of the nanoparticle is fixed via a harmonic spring to a position that travels at constant velocity from the interface to the bulk phase of interest. Although the results shown in Figure 6 cannot be used to estimate the free energy change upon nanoparticle desorption, they can be used to estimate the work required to remove one nanoparticle from the interface.

The results show that the mechanical energy necessary to remove the nanoparticles from the interface grows rapidly as the distance increases. After this quick increase, the mechanical energy reaches a plateau, or grows very slowly as the distance further increases. These results suggest that the interfacial region, as experienced by the nanoparticles, corresponds to the region within which the mechanical energy increases quickly as the distance increases. In correspondence of the plateau, the effective force acting on the nanoparticle approximates the drag force necessary to move the nanoparticle at constant velocity within the bulk of either the aqueous or the organic phases.

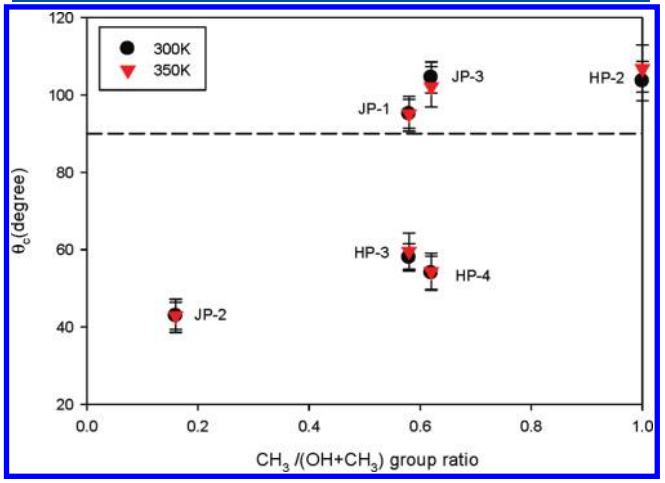

Figure 5. Contact angle θ_c' plotted as a function of the ratio of CH_3 groups versus the total number of surface groups (OH and CH_3) on the nanoparticle surface. The results are obtained at 300 K (filled circles) and 350 K (red triangles). The error bars are obtained as one standard deviation from the average. The dashed line identifies a three-phase contact angle of 90°. When the three-phase contact angle is larger than 90°, w/o emulsions are expected; when the three phase contact angle is less than 90°, o/w ones should form.

Table 4. Desorption Energies Calculated from the Three-Phase Contact Angles Obtained from Simulations (Figure 5) Using Equations 3−5[a]

	HP-2	HP-3	HP-4	JP-1	JP-2	JP-3
E_{Oil} (T = 300 K)	55 ± 15	210 ± 15	225 ± 20	270	355	235
E_{Water} (T = 300 K)	140 ± 20	20 ± 5	15 ± 5	135 ± 15	40 ± 5	140 ± 20
E_{Oil} (T = 350 K)	35 ± 10	145 ± 15	160 ± 15	190	250	170
E_{Water} (T = 350 K)	105 ± 20	16 ± 5	12 ± 5	100 ± 10	30 ± 5	105 ± 15

[a] Energies are expressed in k_BT. The average desorption energy and errors are calculated using the contact angles obtained from 2000 frames of simulation snapshots after the nanoparticles are equilibrated at the interface. For Janus nanoparticles, since we assume $\theta_c = \alpha$, the uncertainties arise from the errors in contact angle measurements for HP-2 (θ_a).

dx.doi.org/10.1021/la200428r |*Langmuir* 2011, 27, 5264–5274

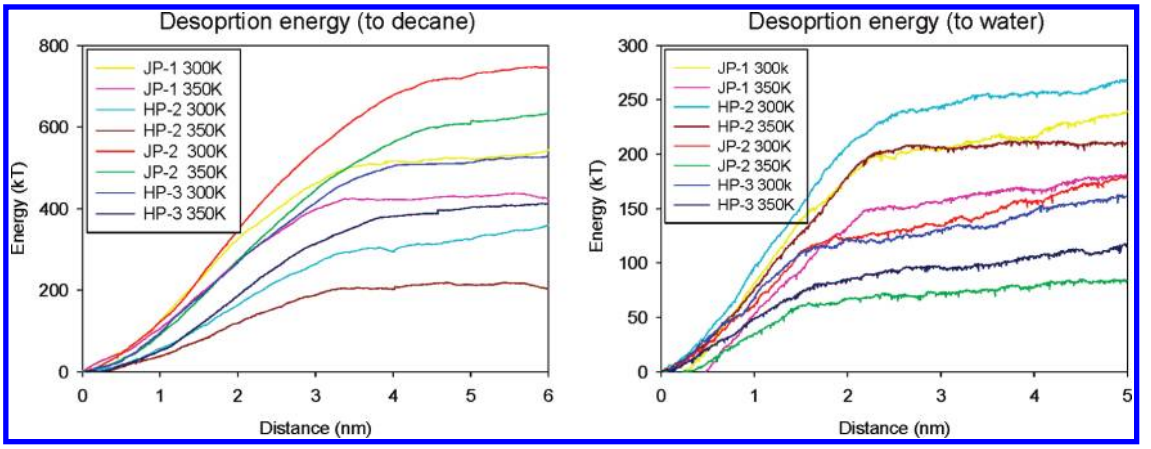

Figure 6. Mechanical energy necessary to remove each of the nanoparticles considered here from the water−decane interface into the water (left panel) or into the organic phase (right panel). The energy is obtained by integrating the force experienced by the nanoparticle over the distance traveled perpendicularly to the interface.

Table 5. Desorption Energies Estimated from Nonequilibrium Simulations (See Methodology for Details)[a]

	HP-2	HP-3	HP-4	JP-1	JP-2	JP-3
E_{Oil} (T = 300 K)	200 ± 35	480	370	470 ± 30	600	415
E_{Water} (T = 300 K)	215 ± 15	80	75	170 ± 40	75	215
E_{Oil} (T = 350 K)	150 ± 40	260	310	330 ± 10	425	305
E_{Water} (T = 350 K)	170 ± 5	60	55	120 ± 20	45	125

[a] Energies are expressed in k_BT. The error is calculated running three independent simulations. Due to time limitations, uncertainties are calculated only for HP-2 and JP-1 nanoparticles. We expect similar uncertainties for the other nanoparticles.

Neither the features of the nanoparticle surface, nor the temperature appear to have a significant effect on the thickness of the effective interfacial region. We estimate that the effective interfacial region has thickness of ∼3.4 and ∼2.2 nm in the oil and aqueous phase, respectively.

The mechanical energy obtained from the simulation results of Figure 6 approximates the energy required to pull one nanoparticle across the interfacial region. Estimates obtained following this procedure overestimate the mechanical desorption energy because they also account for the energy required to overcome hydrodynamic dissipations. An estimate of these resistances has been obtained by considering the slope in the energy profiles of Figure 6 outside of the interfacial region. The energy dissipated because of hydrodynamic effects has been approximated by multiplying the slope of the curves by the thickness of the interfacial region reduced by l to account for the equilibrium position of the nanoparticles (for l, see Figure 3). The results are reported in Table 5.

In general, the mechanical energy necessary to displace one nanoparticle from the interface into the oil phase is significantly larger than the desorption energy calculated using macroscopic considerations (Table 4). Despite these differences, both simulation and macroscopic results agree that all nanoparticles except HP-2 would preferentially desorb from the interface into the aqueous phase. It is possible that increasing the nanoparticles lipophylicity by increasing the length of the hydrophobic moieties (in our simulations short CH_3 groups) as suggested by Glaser et al.[32] will lead to preferential desorption into the organic phase.

Although the difference between results in Table 4 and those in Table 5 is reasonable when the nanoparticles are moved from the interface into the aqueous phase, simulations yield results at least a 150 k_BT larger than thermodynamics estimates when the nanoparticle are pulled from the interface into the oil phase. Visual inspection of simulation snapshots reveals that in the latter circumstances, a "water bridge" is formed while the nanoparticles are pushed into the organic phase, as shown in Figure 7. After the water bridge breaks, some water molecules remain adsorbed on

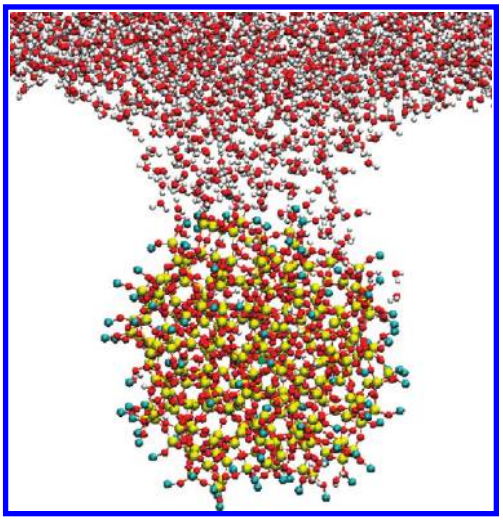

Figure 7. Simulations snapshot illustrating the formation of a water bridge between the HP-2 nanoparticle and the water−decane interface. The nanoparticle is pulled from the interface into the organic phase. Decane is not shown for clarity. Simulations were performed at T = 300 K.

dx.doi.org/10.1021/la200428r |*Langmuir* 2011, 27, 5264–5274

the nanoparticles as they are pulled further into the organic phase. It is likely that the formation of the water bridge and the presence of the adsorbed water molecules are the reasons for the large differences observed. To resolve this artifact, one can use a much slower pulling rate, which, of course, will require much longer simulation times, or implement alternative algorithms such as those proposed by Ranatunga et al.[39] It should however be pointed out that it has been experimentally observed that water molecules tend to adsorb onto a nanoparticle surface, in some cases leading to w/o emulsions when o/w emulsions are expected based on the nanoparticle surface chemistry.[40,41]

Another possibility that might lead to large mechanical desorption energies is due to depletion effects related to the length of decane molecules.[42,43] This contribution, not accounted for in the models of eqs 3−5, is expected to become larger as the molecular weight of the solvent increases.

3.4. Rotational Relaxation. For a number of practical applications, including using nanoparticles at water−oil interfaces as catalyst for the in situ upgrade of biooil to fungible fuels,[3] it is important to understand and, if possible, control the rotation with respect to the oil−water interface. For such purposes we calculated the rotational relaxation autocorrelation function, $C(t)$, for all the nanoparticles considered in this work. $C(t)$ is expressed as

$$C(t) = \frac{1}{2}[3\cos^2\phi_i - 1] \quad (7)$$

For calculating $C(t)$, we identify vectors that move rigidly with the solid nanoparticle. These are obtained by connecting the center of mass of the nanoparticle to selected atoms on its surface. Multiple vectors were used to increase accuracy. The symbol ϕ_i in eq 7 is the angle between the vector just defined at a time t, and the same vector at time $t = 0$. As the time t increases, the nanoparticle rotates, leading to an increase in the angle. Correspondingly, $C(t)$ decreases. The more quickly $C(t)$ decreases, the faster the nanoparticle rotates.

$C(t)$ has been studied with respect to rotations parallel to the direction perpendicular to the oil−water interface (Z axis of the simulation box, see Figure 2), and to the direction parallel to the oil−water interface. When $C(t)$ is calculated with respect to the Z axis, the nanoparticle is effectively rotating within the plane identified by the oil−water interface. When $C(t)$ is calculated with respect to the direction parallel to the interface, the nanoparticle rotates within a plane perpendicular to the interface. The results are shown in Figure 8. Top and bottom panels are for $C(t)$ calculated with respect to the directions parallel and perpendicular to the oil−water interface, respectively.

From the results shown in Figure 8, it is evident that all nanoparticles considered here rotate more easily along the plane of the oil−water interface than along the perpendicular direction. For Janus nanoparticles, this was expected. In fact, as shown by

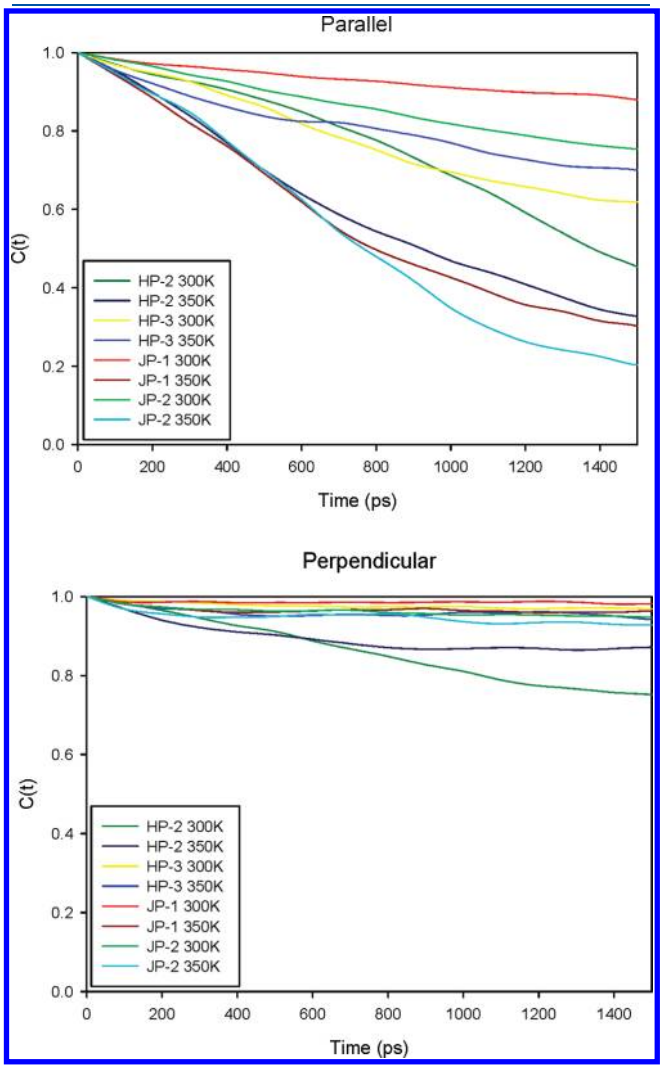

Figure 8. Rotational relaxation autocorrelation functions calculated for the nanoparticles at the water−decane interface.. Top and bottom panels refer to $C(t)$ calculated with respect to the directions parallel and perpendicular to the oil−water interface, respectively.

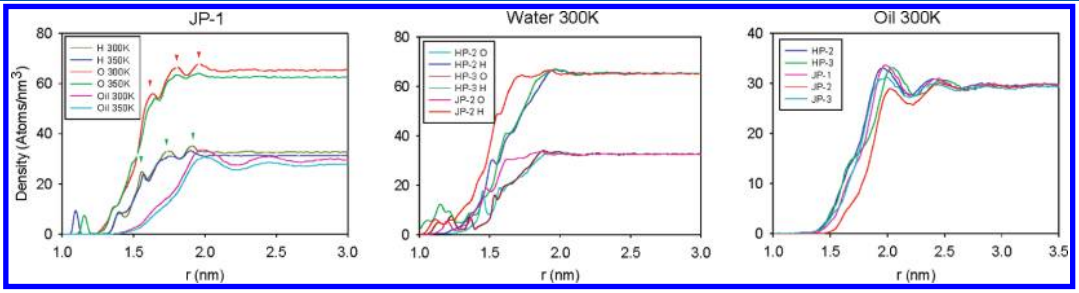

Figure 9. (left) Number density profiles for solvent around JP-1 nanoparticles as a function of the distance from the nanoparticle center. Results obtained at 300 and 350 K are shown. H, O, and C represent hydrogen atoms of water, oxygen atoms of water, and CH_2/CH_3 united-atom groups of decane. (center) Number density profile for water oxygen and hydrogen atoms as a function of the distance from the center of various nanoparticles. Results are obtained at 300 K. (right) Number density profile for CH_2/CH_3 united-atom groups of decane as a function of the distance from the center of the various nanoparticles simulated. Results are obtained at 300 K. See Figure 1 for details concerning each nanoparticle features.

dx.doi.org/10.1021/la200428r |*Langmuir* 2011, 27, 5264–5274

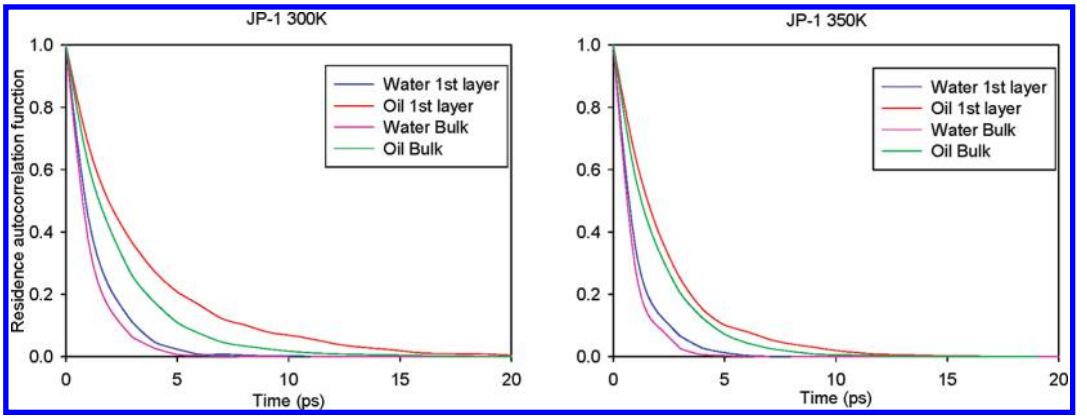

Figure 10. Residence autocorrelation function calculated for decane and water molecules in the first dense layer near the JP-1 nanoparticle and in the bulk at 300 (left panel) and 350 K (right panel).

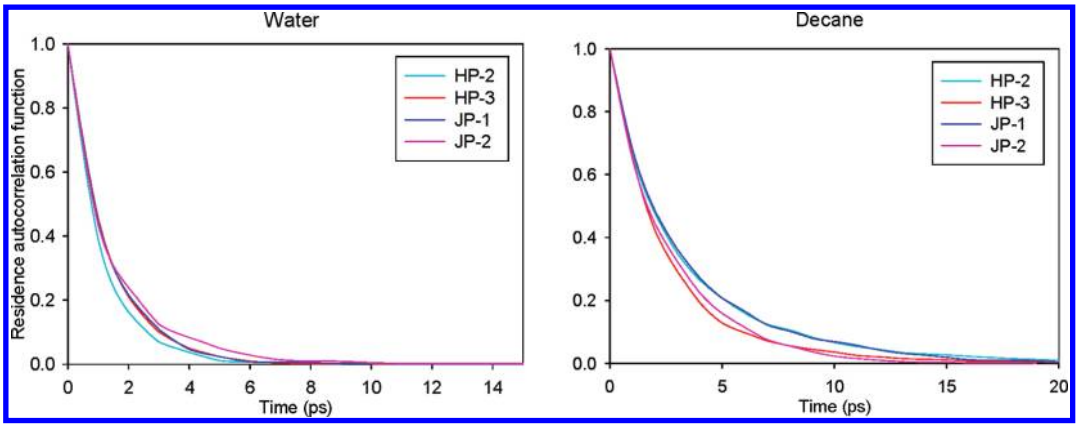

Figure 11. Residence autocorrelation functions for water (left panel) and decane segments (right panel) in the first adsorbed layer obtained near different nanoparticles.

the three-phase contact angle results and by visual analysis of simulation snapshots (not reported for brevity), the hydrophobic portion of the Janus nanoparticles at equilibrium is immersed in the oil phase, while the hydrophilic portion remains in contact with the aqueous phase. On the contrary, when the nanoparticle rotates within the plane perpendicular to the oil−water interface, the hydrophobic groups will enter the aqueous phase and, vice versa, the hydrophilic groups would enter the organic phase. Because of energetic considerations, this rotation will not occur easily, leading to slowly decaying $C(t)$. Similar results obtained for the homogeneous nanoparticles are however surprising. Because the chemical composition of the nanoparticle surface is homogeneous, it was expected that these nanoparticles could rotate along both directions considered. Instead, our results suggest that the rotation within the plane perpendicular to the oil−water interface is an activated process. When the nanoparticle rotates some of the hydrophilic(/hydrophobic) groups, which are at contact with water(/decane), will come in contact with decane(/water) (therefore losing advantageous interactions). Even though this process occurs simultaneously with the opposite (some hydrophilic groups at contact with decane will enter in contact with water upon rotation of the nanoparticle and vice versa), the entire process requires activation and, therefore, is slow. Statistical inaccuracies prevent us from observing clear trends as a function of temperature.

3.5. Density Profiles at the Solvent−Nanoparticle Interface. In Figure 9, we report the atomic density profiles of oxygen and hydrogen atoms of water and of CH_3/CH_2 united atoms of decane, as a function of the distance from the center of the nanoparticles. These calculations were conducted after each nanoparticle reached its equilibrium position at the water−decane interface. Results are shown for simulations conducted at 300 and 350 K.

Previous simulation and experimental results for liquids near flat solid surfaces have shown that liquid molecules form dense layers near solid substrates.[44−52] In agreement, our results show layering of both water and decane at the nanoparticle−solvent interface. However, the peaks observed in Figure 9 are of a significantly less intensity compared to that of peaks typically observed near flat solid substrates. This difference is probably due to the spherical shape of the nanoparticles, which prevents the formation of denser layers, and also to the atomic-scale roughness that characterizes the surface of the nanoparticles simulated here. To this respect, it is instructive to observe that more pronounced layering is observed for decane than for water, probably because the large decane molecule cannot fit the atomic-scale asperities present at the nanoparticle surface.

As shown in Figure 9, left panel, temperature has little effect on the results obtained, although as T increases the intensity of the various density peaks, as well as the bulk density, decrease. The

position of the peaks in all density profiles does not depend on temperature.

Small peaks around $r = 1$ nm at 350 K might be explained by the fact that water molecules at higher temperature penetrate some small surface asperities inaccessible at lower T. By comparing the position of the three peaks of Figure 9 (left panel) in the range $1.5 < r < 2$ nm for the hydrogen (red arrows) and oxygen density profile (green arrows), one finds that the three oxygen peaks are closer to the nanoparticle than for hydrogen. This suggests a preference for interfacial water molecules to point the OH bonds slightly away from the nanoparticle surface. Water molecules show different density profiles around different nanoparticles (see Figure 9, center panel). For JP-2 where the surface in the water phase is fully hydrophilic, the peak highlighted by the red arrows indicates that water molecules are closer to the surface than to HP-2 and HP-3, the surface of which is either fully hydrophobic or partially hydrophobic. Differences in the density profiles suggest different orientation of interfacial water molecules due to different surface properties.

In the case of decane (Figure 9, right panel), it is observed that the position of the first peaks does not differ significantly as a function of the nanoparticle surface properties. The small difference of the first peak position for HP-3 and JP-2 is probably due to the smaller area available for decane to wet the nanoparticles.

3.6. Solvent Residence Time Near the Nanoparticle. A residence correlation function $C_R(t)$ was employed to study the residence time of water and decane molecules in the first dense layer near the nanoparticles (the first peak in the solvent density profile). Due to the broad peaks shown in Figure 9, we set the position of the first layer at a fixed value: 1.9 nm from the center of the nanoparticles for water and 2.0 nm for decane. Any water molecule whose oxygen was found within a computational bin of 0.1 nm in thickness centered on the 1.9 nm radius was considered as contact water. Any methyl group whose center was found within a computational bin of thickness 0.2 nm centered on the 2.0 nm radius was considered contact methyl. The residence time of liquid molecules in the bulk is measured at 3.5 nm from the center of nanoparticles. In the case of decane, the residence time was calculated for individual methyl segments. The residence correlation functions were calculated as

$$C_R^w(t) = \frac{\langle O_w(t)O_w(0)\rangle}{\langle O_w(0)O_w(0)\rangle}; \quad C_R^d(t) = \frac{\langle O_D(t)O_D(0)\rangle}{\langle O_D(0)O_D(0)\rangle} \qquad (8)$$

In eq 8, angular brackets denote ensemble averages. Superscripts w and d denote water and decane, respectively. The terms $O_w(t)$ and $O_D(t)$ describe whether an oxygen atom of water or a methyl group of decane, respectively, is or is not in the first interfacial layer considered at time t. The correlation functions decay from 1 to 0 as time elapses. The more slowly the correlation decays, the longer the molecules stay in the interfacial area. The residence time could be estimated from results for the residence autocorrelation function, following, for example, the method described in prior works.[44,50]

As shown in Figure 10, residence autocorrelation functions for both water and decane decay more slowly when the molecules are near the nanoparticles that when they are in the bulk. This observation is in qualitative agreement with results obtained near flat silica surfaces.[50] Our results also show that the residence time for both water and decane at the nanoparticle−liquid interface decrease significantly when temperature is raised from 300 to 350 K.

For different nanoparticles, as shown in Figure 11, the residence autocorrelation functions for both decane and water are only slightly influenced by the nanoparticle surface properties.

4. CONCLUSIONS

We have used molecular dynamics simulations to investigate the influence of the surface chemistry of silica nanoparticles of 3 nm diameter on their properties at the water−decane interface. The nanoparticle surface chemistry was altered by systematically varying the surface groups. Methyl groups (CH_3) were used as representative hydrophobic sites, while hydroxyl groups (OH) were used as representative hydrophilic groups. The overall hydrophobicity of the nanoparticle was controlled by the ratio between CH_3 and OH groups present at the interface. Nanoparticles with equal overall chemical composition were prepared with different distribution of the various surface groups, leading to homogeneous vs Janus nanoparticles. The properties of interest include water−decane interfacial tension in the presence of the various nanoparticles, three-phase contact angles, desorption energy, nanoparticle rotational relaxation, and residence time for water and decane at contact with the nanoparticle−liquid interface. Temperature changes, in the range 300 to 350 K, were found to only slightly affect all the results discussed.

Our models predict values for the water−decane surface tension that agree with experiments. The nanoparticle completely covered with −OH groups, in qualitatively agreement with experiments, preferentially partitions to the water phase and does not reside at the water−decane interface. The other nanoparticles only slightly affect the surface tension, which is also in agreement with a number of experimental data.

As the surface hydrophobicity of the nanoparticle increases (quantified with the density of $-CH_3$ groups), the three-phase contact angle at the decane−water interface increases. Contact angles obtained for all nanoparticles considered herein are always less than ∼105°. For nanoparticles with equal overall surface chemical composition, it was found that when the surface groups (−OH or $-CH_3$) are randomly distributed on the nanoparticle surface (homogeneous nanoparticles) contact angles are typically less than 90°. When the surface groups are distributed on the nanoparticle surface to generate Janus nanoparticles, the contact angles can be larger than 90°. These results are important because contact angles smaller or larger than 90° are expected to stabilize o/w and w/o Pickering emulsions, respectively. When forced to desorb from the interface, all nanoparticles preferentially partition to the water phase. When pulled into the oil phase, the nanoparticles tend to carry along water molecules adsorbed on their surface, a phenomenon observed experimentally.

All the nanoparticles, Janus and homogeneous, when adsorbed at the water−decane interface rotate more freely along the plane parallel to the interface than along the plane perpendicular to it. Both water and decane form rather dense atomic layers at contact with all the nanoparticles. It was found that the molecules belonging to these contact layers show delayed dynamics compared to those found in the bulk. The nanoparticle surface properties affect these observations, but only to a limited extent.

The results presented are useful for deriving coarse-grained models that could be used to study emergent behavior of both homogeneous and Janus nanoparticles at water−oil interfaces.

■ ASSOCIATED CONTENT

Supporting Information. Calculation of orientation of decane chains within the thin film. This material is available free of charge via the Internet at http://pubs.acs.org.

■ AUTHOR INFORMATION

Corresponding Author
*E-mail: astriolo@ou.edu.

■ ACKNOWLEDGMENT

This work was supported, in part, by NSF award no. CBET-1033129 to the University of Oklahoma and by NSF EPSCoR award no. EPS0814361 to the State of Oklahoma. Generous allocations of computing time were provided by the OU Supercomputing Center for Education and Research (OSCER) and by the National Energy Research Scientific Computing Center (NERSC) at Lawrence Berkley National Laboratory.

■ REFERENCES

(1) Huber, G. W.; Iborra, S.; Corma, A. *Chem. Rev.* **2006**, *106* (9), 4044–4098.
(2) Huber, G. W.; Dumesic, J. A. *Catal. Today* **2006**, *111* (1−2), 119–132.
(3) Crossley, S.; Faria, J.; Shen, M.; Resasco, D. E. *Science* **2010**, *327* (5961), 68–72.
(4) Shen, M.; Resasco, D. E. *Langmuir* **2009**, *25* (18), 10843–10851.
(5) Binks, B. P.; Lumsdon, S. O. *Langmuir* **2000**, *16* (23), 8622–8631.
(6) Binks, B. P. *Curr. Opin. Colloid Interface Sci.* **2002**, *7* (1−2), 21–41.
(7) P. Binks, B.; O. Lumsdon, S. *Phys. Chem. Chem. Phys.* **1999**, *1* (12), 3007–3016.
(8) Binks, B. P.; Fletcher, P. D. I. *Langmuir* **2001**, *17* (16), 4708–4710.
(9) Cayre, O. J.; Paunov, V. N. *Langmuir* **2004**, *20* (22), 9594–9599.
(10) Mohammadi, R.; Amirfazli, A. *J. Disp. Sci. Technol.* **2004**, *25* (5), 567–574.
(11) Yakubov, G. E.; Vinogradova, O. I.; Butt, H. J. *J. Adhes. Sci. Technol.* **2000**, *14* (14), 1783–1799.
(12) Litton, D. A.; Garofalini, S. H. *J. Appl. Phys.* **2001**, *89* (11), 6013.
(13) Zhuravlev, L. T. *React. Kinet. Catal. Lett.* **1993**, *50* (1−2), 15–25.
(14) Cygan, R. T.; Liang, J. J.; Kalinichev, A. G. *J. Phys. Chem. B* **2004**, *108* (4), 1255–1266.
(15) Martin, M. G.; Siepmann, J. I. *J. Phys. Chem. B* **1998**, *102* (14), 2569–2577.
(16) Berendsen, H. J. C.; Grigera, J. R.; Straatsma, T. P. *J. Phys. Chem.* **1987**, *91* (24), 6269–6271.
(17) Brodka, A.; Zerda, T. W. *J. Chem. Phys.* **1996**, *104* (16), 6319–6326.
(18) Allen, M. P.; Tildesley, D. J. *Computer Simulation of Liquids*; Oxford University Press: Oxford, UK, 2004.
(19) Essmann, U.; Perera, L.; Berkowitz, M. L.; Darden, T.; Lee, H.; Pedersen, L. G. *J. Chem. Phys.* **1995**, *103* (19), 8577–8593.
(20) Lindahl, E.; Hess, B.; van der Spoel, D. *J. Mol. Model.* **2001**, *7* (8), 306–317.
(21) Hess, B.; Kutzner, C.; van der Spoel, D.; Lindahl, E. *J. Chem. Theory Comput.* **2008**, *4* (3), 435–447.
(22) Berendsen, H. J. C.; Vanderspoel, D.; Vandrunen, R. *Comput. Phys. Commun.* **1995**, *91* (1−3), 43–56.
(23) Van der Spoel, D.; Lindahl, E.; Hess, B.; Groenhof, G.; Mark, A. E.; Berendsen, H. J. C. *J. Comput. Chem.* **2005**, *26* (16), 1701–1718.
(24) Berendsen, H. J. C.; Postma, J. P. M.; Vangunsteren, W. F.; Dinola, A.; Haak, J. R. *J. Chem. Phys.* **1984**, *81* (8), 3684–3690.
(25) Ikeda, S.; Takahara, Y. K.; Ishino, S.; Matsumura, M.; Ohtani, B. *Chem. Lett.* **2005**, *34* (10), 1386–1387.
(26) Luo, M. X.; Mazyar, O. A.; Zhu, Q.; Vaughn, M. W.; Hase, W. L.; Dai, L. L. *Langmuir* **2006**, *22* (14), 6385–6390.
(27) Alejandre, J.; Rivera, J. L.; Mora, M. A.; de la Garza, V. *J. Phys. Chem. B* **2000**, *104* (6), 1332–1337.
(28) Goebel, A.; Lunkenheimer, K. *Langmuir* **1997**, *13* (2), 369–372.
(29) Zeppieri, S.; Rodriguez, J.; de Ramos, A. L. L. *J. Chem. Eng. Data* **2001**, *46* (5), 1086–1088.
(30) Okubo, T. *J. Colloid Interface Sci.* **1995**, *171* (1), 55–62.
(31) Vignati, E.; Piazza, R.; Lockhart, T. P. *Langmuir* **2003**, *19* (17), 6650–6656.
(32) Glaser, N.; Adams, D. J.; Boker, A.; Krausch, G. *Langmuir* **2006**, *22* (12), 5227–5229.
(33) Shi, L.; Tummala, N. R.; Striolo, A. *Langmuir* **2010**, *26* (8), 5462–5474.
(34) Fernandes, P. A.; Cordeiro, M.; Gomes, J. *J. Phys. Chem. B* **1999**, *103* (42), 8930–8939.
(35) Jorge, M.; Natalia, M.; Cordeiro, D. S. *J. Phys. Chem. C* **2007**, *111*, 17612–17626.
(36) Szori, M.; Tobias, D. J.; Roeselova, M. *J. Phys. Chem. B* **2009**, *113* (13), 4161–4169.
(37) Giovambattista, N.; Debenedetti, P. G.; Rossky, P. J. *J. Phys. Chem. C* **2007**, *111* (3), 1323–1332.
(38) Jiang, S.; Granick, S. *J. Chem. Phys.* **2007**, *127* (16), No. 161102.
(39) Udayana Ranatunga, R. J. K.; Kalescky, R. J. B.; Chiu, C.-c.; Nielsen, S. O. *J. Phys. Chem. C* **2010**, *114* (28), 12151–12157.
(40) Binks, B. P.; Lumsdon, S. O. *Phys. Chem. Chem. Phys.* **2000**, *2* (13), 2959–2967.
(41) Binks, B. P.; Rodrigues, J. A. *Langmuir* **2003**, *19* (12), 4905–4912.
(42) Asakura, S.; Oosawa, F. *J. Polym. Sci.* **1958**, *33* (126), 183–192.
(43) Oosawa, F.; Asakura, S. *J. Chem. Phys.* **1954**, *22* (1), 1.
(44) Argyris, D.; Tummala, N. R.; Striolo, A.; Cole, D. R. *J. Phys. Chem. C* **2008**, *112* (35), 13587–13599.
(45) Striolo, A.; Chialvo, A. A.; Cummings, P. T.; Gubbins, K. E. *Langmuir* **2003**, *19* (20), 8583–8591.
(46) Striolo, A.; Gubbins, K. E.; Gruszkiewicz, M. S.; Cole, D. R.; Simonson, J. M.; Chialvo, A. A. *Langmuir* **2005**, *21* (21), 9457–9467.
(47) Lopes, P. E. M.; Murashov, V.; Tazi, M.; Demchuk, E.; MacKerell, A. D. *J. Phys. Chem. B* **2006**, *110* (6), 2782–2792.
(48) Gordillo, M. C.; Marti, J. *J. Chem. Phys.* **2002**, *117* (7), 3425–3430.
(49) Wander, M. C. F.; Clark, A. E. *J. Phys. Chem. C* **2008**, *112* (50), 19986–19994.
(50) Argyris, D.; Cole, D. R.; Striolo, A. *J. Phys. Chem. C* **2009**, *113* (45), 19591–19600.
(51) Argyris, D.; Cole, D. R.; Striolo, A. *Langmuir* **2009**, *25* (14), 8025–8035.
(52) Argyris, D.; Cole, D. R.; Striolo, A. *ACS Nano* **2010**, *4* (4), 2035–2042.